The Gemini MCAO System GeMS: nearing the end of a lab-story

B. Neichel[a], F. Rigaut[a], M. Bec[a], M. Boccas[a], F. Daruich[a], C. D'Orgeville[a], V. Fesquet[a], R. Galvez[a], A. Garcia-Rissmann[a], G. Gausachs[a], M. Lombini[b], G. Perez[a], G. Trancho[a], V. Upadhya[a] and T. Vucina[a]

[a]Gemini Observatory, c/o AURA, Casilla 603, La Serena, Chile;
[b]INAF - Osservatorio Astronomico di Bologna- Via Ranzani, 1 - 40127 Bologna - Italy

ABSTRACT

GeMS (the Gemini Multi-conjugated adaptive optics System) is a facility instrument for the Gemini-South telescope. It will deliver a uniform, diffraction-limited image quality at near-infrared (NIR) wavelengths over an extended FoV or more than 1 arcmin across. GeMS is a unique and challenging project from the technological point of view and because of its control complexity. The system includes 5 laser guide stars, 3 natural guide stars, 3 deformable mirrors optically conjugated at 0, 4.5 and 9km and 1 tip-tilt mirror. After 10 years since the beginning of the project, GeMS is finally reaching a state in which all the subsystems have been received, integrated and, in the large part, tested. In this paper, we report on the progress and current status of the different sub-systems with a particular emphasis on the calibrations, control and optimization of the AO bench.

Keywords: Multi Conjugated Adaptive Optics, Calibration, Diagnostics, Integration and test, characterization

1. INTRODUCTION

GeMS (the Gemini Multi-conjugated adaptive optics System) is a facility instrument. Due to its complexity, we usually divide it into sub-systems, the main ones -in the scope of this paper- being the laser, the Beam Transfer Optics (BTO), the Laser Launch Telescope (LLT) and the AO bench (Canopus). All these sub-systems are interacting together through control loops and offloads. Fig. 1 shows the overall GeMS diagram and illustrates the (complex) interactions required between the different sub-systems. A detailed description of each sub-system can be found in previous papers.[1–5] In short, a 50W laser is split in 5x10W beacons to produce the 5 laser guide stars (LGS) placed on the sky at the corner and center of a 60 arcsec square. These five LGS are seen by five, 16x16 subapertures, Shack-Hartmann wavefront sensors (WFS). The 2040 slope measurements are used to compute the MCAO high-order correction, correction provided at 800Hz by three deformable mirrors conjugated to 0, 4.5 and 9km and totaling 917 actuators. Besides that, up to three either visible or NIR natural guide stars (NGS) provide the measurements for the compensation of the tip-tilt and anisoplanatic modes. The tip-tilt compensation is done by a tip-tilt mirror (TTM) while the tilt-anisoplanatic modes are compensated by a combination of quadratic modes on DM0 and DM9. In addition, a fraction of the NGS light is directed toward a Slow Focus WFS (SFS), which control the LGS WFS zoom. On top of this main scheme, several secondary loops and offloads are implemented all along the path (see Fig. 1).

In order to simplify the documentation effort we have developed a common and simple scheme based on a Wiki plus Blog architecture. The Blog is a very convenient way to keep a day to day trace of the project progress. Basically, every new results/progress/issues are blogged. This is also a friendly way to keep all the team informed of the sub-components status. We started the MCAO blog in July 2007, and after 3 years of use it's totaling 529 posts (at the time of the conference). This represents an average of 15 posts per month. The Wiki is used to keep all the weekly meeting notes, procedures and documentation. The MCAO wiki has started in August 2008 (22 months of use) and it's totaling 530 pages currently (150 if we exclude meeting reports). We have an average of 120 page edit per month, and more than 700 page view per month !

GeMS is currently undergoing integration and test with a first light planned early 2011. Below we report on the current status of the main components.

Send correspondence to bneichel@gemini.edu or frigaut@gemini.edu

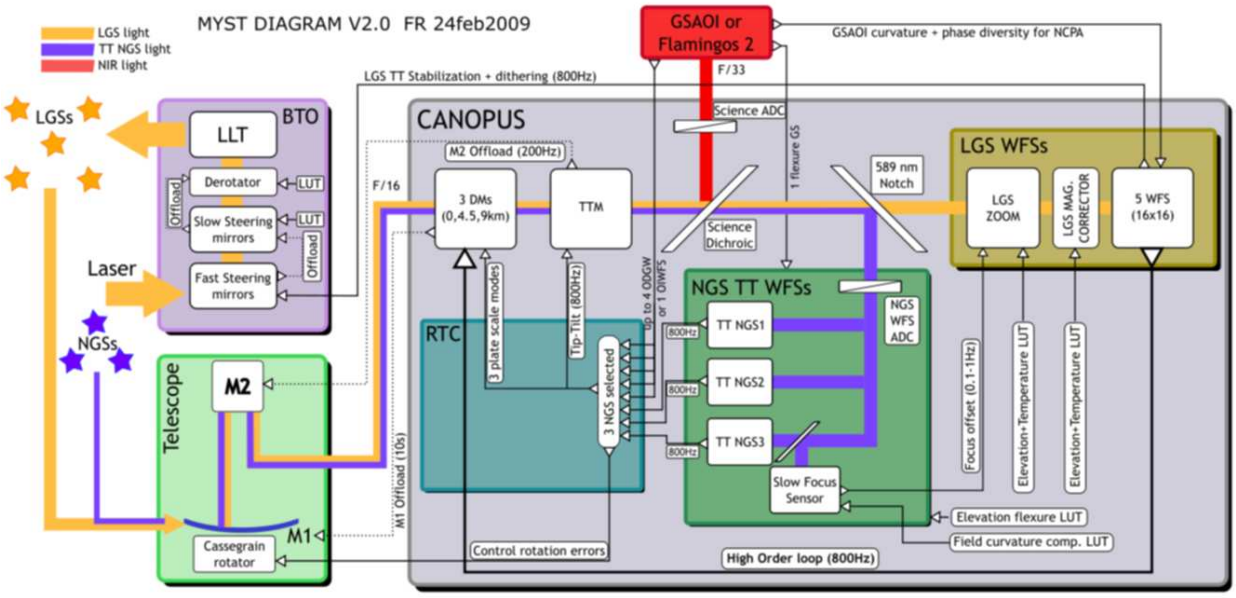

Figure 1. GeMS synaptic diagram. The main components represented here are the Laser, the Beam Transfer Optics (BTO) and Canopus (the AO bench).

1.1 Canopus

Canopus is the AO bench of GeMS. The integration of the opto-mechanical components and their characterization continues its way in a lab facility at the Gemini South base facility in Chile. A major engineering effort was started last year to re-design the thermal enclosures of the Canopus electronics, particularly to manage the heat load of the Deformable Mirror Electronics (DME), 2900W accounting for about 70% of the total 4100 W heat waste to be extracted from the instrument. The DME components are also particularly sensitive to over temperatures and called for a complete and thorough redesign using new heat exchangers, high performance DC fans, compressed dry air, active valves and new telemetry to monitor the enclosure environment, electronics temperatures and any risk of condensation. Other critical aspects including vibrations and restriction due to the compact envelope of Canopus had to be considered. The new design was completed and passed critical design review in December 2009, fabrication and assembly completed in April 2010 (see Fig.2 (left-side) for a picture of the new cooling system). The installation and testing is getting close to completion and expected to finish by the end of June 2010. Preliminary acceptance tests have shown the new system will meet the cooling specifications we had set with some margin[6] .

While this effort was taking place, we temporarily patched the system to allow parallel work for AO characterization. The opto-mechanical performance of the NGS WFS probes[3] was characterized at different elevation and temperature. We were able to uncover some issues with repeatability and plan to address them. We determined the optical throughput of the NGS WFS path was below specification and started to design a replacement using new set of pyramids, fibers and fiber coupling. Although a limiting factor for performance on fainter guide stars, we plan to pursue commissioning of Canopus using brighter natural guide stars, and retrofit the new probes during next winter 2011.

The functionality of the Real Time Controller (RTC) was thoroughly tested, including offloads and interactions with other system in GeMS: Laser Fast Steering Mirrors, telescope M1 optics, telescope M2 offloads. Optimization algorithms have been developed using the software framework presented in a companion paper[7] or embedded in the RTC DSP digital signal processors.

Late November 2009, a major fault occurred with the DME 4.5 because of overheating and prevented us to use the bench further for AO work that require the High-Order (HO) loop closed. Following this major incident, our effort shifted to raise the priority for cooling redesign within the engineering team, and develop the high

level aspect of GeMS software particularly smart sequencing and simulations[7] . We also took that opportunity to send back one of Canopus deformable mirror (DM0) that had one dead actuator, surface defects and coating tarnish for repair, repolishing and recoating in France at the Cilas manufacturer. DM0 is expected to come back in Chile around September 2010, by which time we will have the DME thoroughly checked, a properly engineered thermal solution, and all the elements to reach the conclusion of the instrument lab-story.

1.2 Laser

Back in September 2005, a single contract to design and fabricate one 20W and one 50W sodium (589nm) guidestar lasers for use at the W. M. Keck, and Gemini South Observatories respectively, was placed with Coherent Technologies Inc. (CTI). The technology, based on diode-pumped solid-state frequency summing of 1064 and 1319 Nd:YAG lasers[8] , was largely based on experience gained with the 14W Guidestar laser built by the same company and installed on the Gemini North telescope in Hawaii in May of that year[9,10] . A detailed description of the GS and Keck laser design, fabrication and performance can be found in previous papers[11,12] .

Various issues, including technical difficulties in procuring the material for the waveguide amplifier modules (WAMs) for the infra-red lasers and various resource issues following the merging of CTI into Lockheed Martin Coherent Technologies (LMCT), delayed the delivery of the two laser systems a couple of years beyond schedule. Eventually in the fall of 2009, the Keck laser was delivered to the W. M. Keck Observatory in Hawaii and installed on the Keck I telescope where it typically performed at the 30-40W output power level with good beam quality (M^2 ~1.2) and reliable wavelength locking on the peak of the sodium D2 line. During factory acceptance testing at the LMCT facility in Louisville, Colorado, in January 2010, the Gemini South (GS) laser successfully demonstrated its ability to perform at the 55-65W level with good beam quality (M^2 ~1.2) and stable wavelength lock. The GS laser was subsequently shipped to Chile and delivered to the Cerro Pachon summit in March 2010.

Shortly after the GS laser went through post-delivery functional testing in the instrument laboratory clean room in April 2010 (see Fig.2), multiple computer crashes prevented completion of the one remaining test, that of the Laser Control System (LCS) reliability. Troubleshooting efforts resulted in shipping the GS laser PXI controller back to its manufacturer, National Instrument, for repair. The computer hard drive was replaced, and the PXI controller was reinstalled in the GS laser electronics enclosure in mid-June 2010. Software testing will still be on-going at the time of this conference (early July 2010). Pending successful completion of the LCS testing, the GS laser should be installed on the telescope in mid-July. The laser bench and its electronics enclosure are located inside a Laser Service Enclosure (LSE), an 8x2m clean room built in-house on an extension of the telescope elevation platform (a Nasmyth focus for other telescopes). The LSE was described by Cavedoni et al[13] and was installed on the telescope in April 2009 (see Fig.2). It is now being tested for temperature stability and cleanliness. Our requirements are quite tight in order to minimize laser cavity realignment throughout the night and the year: ±0.5degC/h and ±2degC year-round. The Laser Bench Stabilization System to compensate differential vibrations between the telescope and the laser (mounted on separate foundations) will be done with a closed loop system based on a Position Sensing Device and a Fast Piezo Tip-tilt mirror in the BTO optical train.

Our ambitious laser commissioning schedule plans for laser first light on the sky at the end of July, albeit not at the 50W output power level. We anticipate that the GS laser will require a minimum of five weeks of alignment and optimization work in its final working environment in the LSE on the GS telescope (see Fig.2) before it delivers its specified performance in terms of output power (P>50W), beam quality (M^2 <1.4), wavelength lock (±100MHz around the peak of the sodium D2 line), and overall system stability.

1.3 BTO

BTO is the beam transfer optics system of GeMS[2] . The construction and integration proceeded during 2009 and early 2010, adopting a modular approach. Currently BTO is 90% installed on the telescope and the remaining elements are planned to be installed in Late June, early July 2010. A dummy 594nm alignment laser was installed in the laser Service Enclosure in lieu of the 50W 589nm laser. Relay optics to the Secondary Support Structure are installed and have been aligned to relay the beam from the fixed laser room onto the telescope elevation axis and then along the telescope truss to the top end ring where a beamsplitter assembly transforms the incoming beam into 5 beams of equal power and polarization. The laser launch telescope and the BTO optical bench

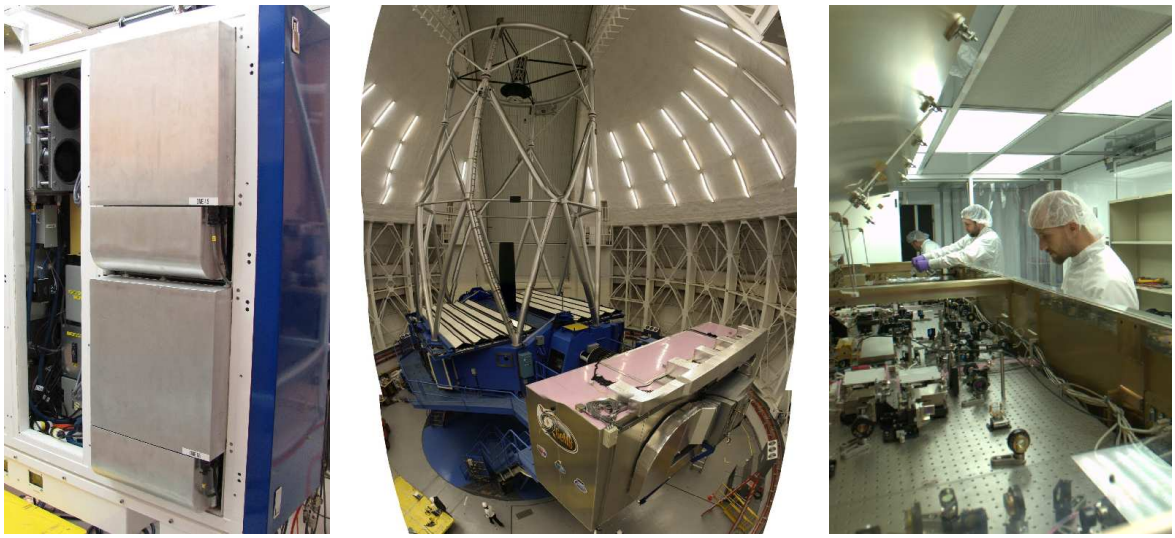

Figure 2. *Left:* New cooling system for the DM electronic recently installed on CANOPUS. *Middle:* Laser Service Enclosure mounted on Gemini south telescope. *Right:* Post-delivery inspection of the GS laser system in the Cerro Pachon instrument laboratory clean room.

(among other things, shaping the beams as the LGS constellation on the sky) have been tested together and are being installed in June 2010 to complete an end-to-end alignment at safer alignment laser power. The first acceptance test on the sky will consist of aligning the optical bench (BTOOB) and LLT for which 2 nights of telescope engineering time have been scheduled. Three weeks later, end of July or beginning of August 2010, we will start the first tests with the laser system and propagate on the sky. Weather permitting, the BTO will be fully commissioned by the end of August 2010. The Laser Guide Star Facility (LGSF) will be fully commissioned by November 2010.

2. CALIBRATIONS AND CALIBRATION TOOLS OF THE AO BENCH

A first description of the calibrations and calibration tool of the AO bench can be found in previous papers[4,5] . In the following, we focus on key calibrations and results that have been obtained recently. All our calibration sequences are implemented through MYST (MCAO Yorick Smart Tool), a yorick+python+GTK software package developed in-house. Myst allows multiple users to control and monitor the bench remotely over the network. More details on Myst are presented in a companion paper[7] .

2.1 Non Common Path Aberrations (NCPA)

In an MCAO system, the static aberrations have to be compensated simultaneously over the entire output focal plane. Recently, we were able to achieve this goal by using a Diagnostic WFS (DWFS, 24x24SH) located in the science focal plane.[4] The DWFS can patrol a large fraction of the science focal plane. Results have been encouraging: in three iterations, we reach a H band static Strehl ratio of 96%±1% (see left side of Fig.3). All Strehl ratio were measured by the DWFS using 120 Zernike modes. Two iterations are needed to compensate the high order aberrations, and a third one is used to control only astigmatism, which make most of the initial aberrations. Additional iterations do not provide further improvements, which tends to indicate the presence of 50nm rms aberrations that can not be corrected, probably because it is located outside of the altitude range that can be compensated by the system (0-9km).

When CANOPUS will be installed on the telescope, we will use GSAOI –a NIR imager dedicated to MCAO– to measure and compensate for the NCPA. Phases estimates will be derived simultaneously at many points in the field of view (from several calibration stars) by using a phase diversity algorithm, possibly completed by extra-focal –in the curvature sense- images. The phase diversity algorithm (called 'OPRA' for OTF based

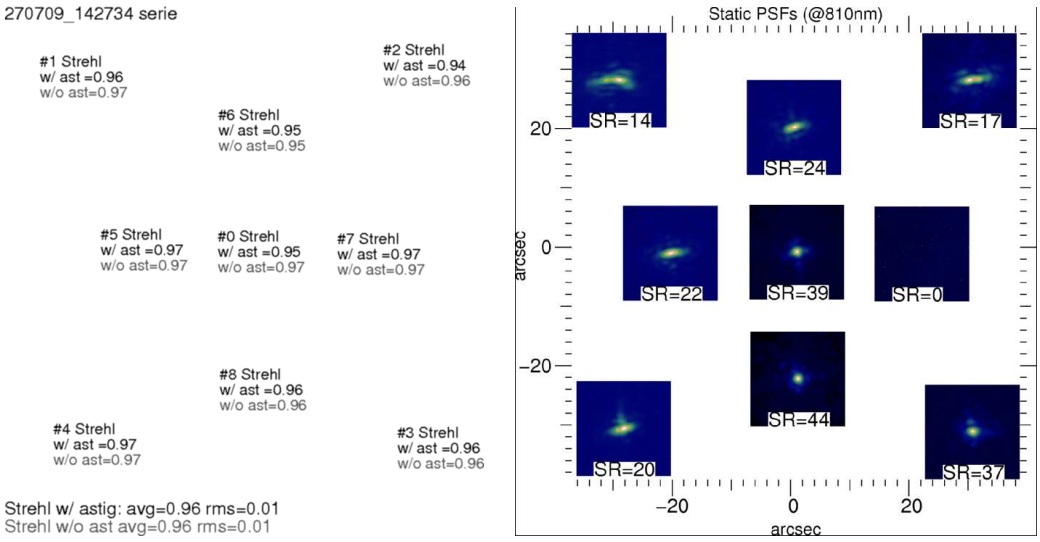

Figure 3. *Left:* H band static Strehl in the field after three iterations of NCPA compensation with the DWFS. *Right:* Raw PSFs acquired with the imaging CCD camera at 810nm over the field when no NCPA compensation is applied. SR are given at 810nm.

Phase Retrieval Algorithm) has been developed in-house, with collaboration from Damien Gratadour. In order to start the validation and calibration of this algorithm we have interfaced an imaging CCD camera in parallel to the DWFS presented above. Raw PSFs acquired in the field are shown in Fig.3 (right-side). First phase estimations/compensations were obtained on the bench last November, unfortunately the conjunction of a DM electronic issue, bench shutdown and DM0 sent back for repair (see1.1) stopped us before we were able to reproduce the results obtained with the DWFS. Therefore we continued the preparation work by using a full simulator of the AO bench and the RTC (see Rigaut et al.[7] companion paper for the full description of this simulator). In particular, we began the calibration work required to evaluate the conversion factors between the output of Opra and the LGS WFS slope offsets. The idea would be to calibrate the system such as we could recycle all the NCPA tomography algorithms that has been developed as presented above. To do so, we build an interaction matrix between the LGS WFS slopes offsets and the reconstructed phase given by Opra (e.g. see Sauvage et al.[14]). Opra's estimated phase is based on a modal approach (either Zernike or KL). So we construct this interaction matrix by (1) projecting Opra modes on the LGSWFS slopes, (2) closing the loop with these offsets, (3) acquire focal and extra-focal images and (4) retrieve the aberrations with Opra. In Fig.4 (top) we illustrate the output given by Opra for one step of this process as well the resulting interaction matrix as measured for the first 21modes (bottom). As one can see the relation between the modes introduced and retrieved is quasi one to one, the interaction matrix is close to be fully diagonal. By using the invert of this matrix we were able (still with the simulator) to go from 24% SR (H Band) to 95% in a single, arbitrary direction in one iteration. Additional iterations do not provide further improvements, which indicates that they are still some calibration and linearity issues that would need to be understood.

2.2 Tip-Tilt and High-Order transfer functions

We calibrated the High-Order (HO) and Tip-Tilt (TT) loop behavior versus transfer function models. For the TT loop, this work was motivated by the need to obtain an accurate model of the loop transfer functions to use in the loop gain optimization routines. For the HO loop, we would like to characterize and monitor the DMs actuators health.

For both the TT and HO loop, the procedure is similar: we record open loop and close loop circular buffers of the error signal, while operating under noise-only conditions. We then compute the Error Transfer Function (ETF) by normalizing the close-loop transfer functions with the open-loop ones. We repeated the measurements

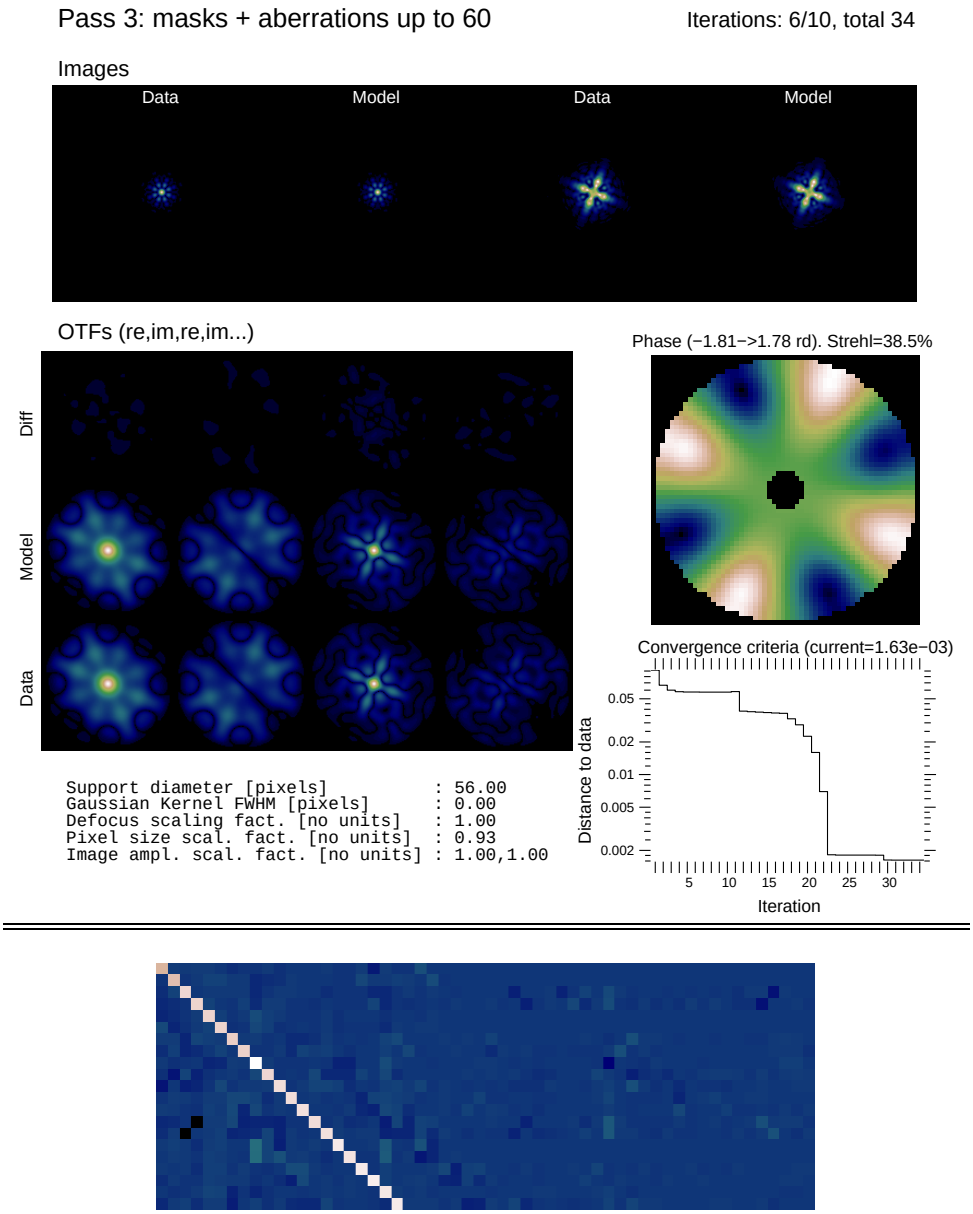

Figure 4. *Top:* Output given by Opra, the phase diversity algorithm, when only one KL mode is introduced as NCPA. *Bottom:* Interaction matrix (obtained in simulation) between the LGS WFS slopes offsets (KL modes) and the modes measured by Opra. In this example 21modes (y-axis) were introduced one-by-one as NCPA. For each one, the phase is estimated over 60modes (x-axis).

for different loop gains (between 0.1 to 0.7) and different loop rates (from 100Hz to 800Hz). Finally, we fitted the ETF with a simple model that takes into account the delays in the loop[15] .

2.2.1 High-Order results

In Fig. 5 we show the results obtained for the HO loop closed with DM0 only. The experimental curves (in black) have been obtained by taking the median of all the actuators. The fitted curves (in red) are obtained with only the gain as free parameter (fitted gains are indicated on the plots). As a first results, we see that the models are in excellent agreement with the experimental data. The fitted gains are different of the set gains by a constant factor (about 0.8). This is probably due to a scaling error in the command matrix or an error in the centroid

gains. From the fits, we found a calculation time of 1.3ms in good agreement with the RTC specifications. Indeed, this lag time is divided between the read-out time (1.25ms) and the remaining command computation time after the last WFS pixel has been received (an additional 0.05ms according to RTC acceptance tests). We also found that the mirror response time is negligible, which is what we expected from the manufacturer data. We repeated these measurements for DM4.5 and DM9, and the results are in excellent agreement with the ones for DM0.

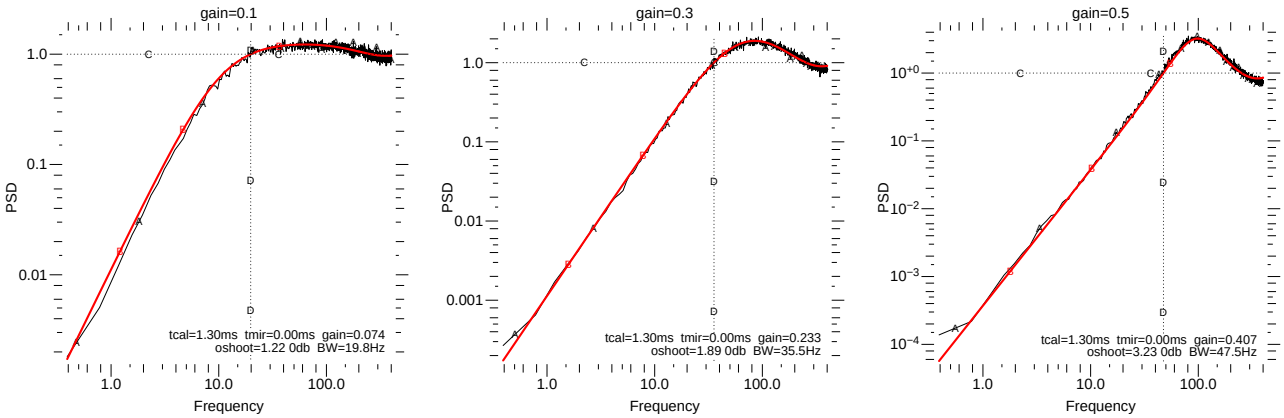

Figure 5. Three examples ETF measured and fitted for DM0.

In Fig. 6 we show a bandwidth map of the actuators of DM0, DM4.5 and DM9. We obtained these maps by computing the ETF for each actuators independently. These maps are a very straightforward and easy way to monitor the actuators health. For instance, we found from these maps that 2 actuators of DM0 were having a very low bandwidth. We are implementing a scheme to run these tests automatically in order to monitor the actuators health on a regular basis.

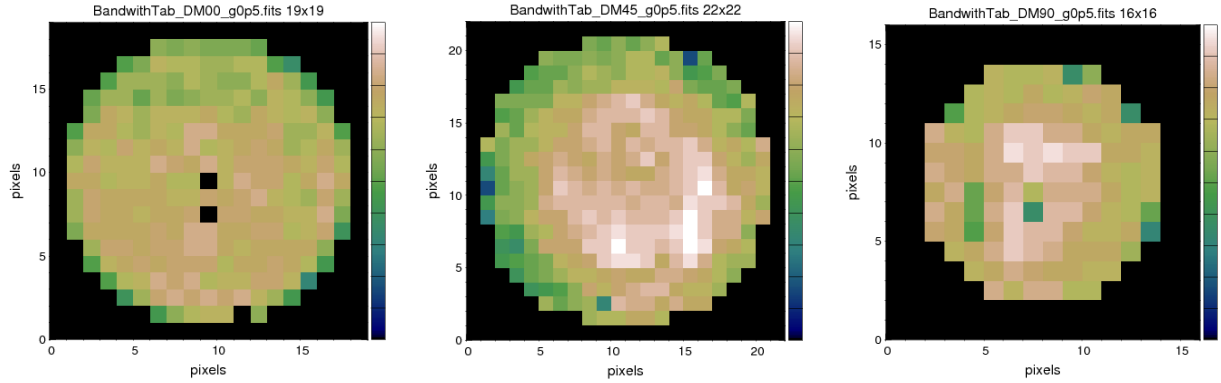

Figure 6. Bandwidth maps for our 3DMs, respectively from left to right: DM0, DM4.5 and DM9. The scale is the same for the 3DMs, from 35Hz to 60Hz. These maps were obtained with a similar set gain of 0.5 for the 3DMs. DM0 shows 2 actuators with a very low bandwidth (the central actuator is a slave ones). Minimum, maximum and rms bandwidths are respectively: [23 (43), 56 (56), 3.6 (2.6)]Hz for DM0 (values in parenthesis are with the 2 bad actuators removed); [39, 61, 3.9]Hz for DM4.5 and [43, 59, 3.0]Hz for DM9.

The current design of the RTC allows us to implement more sophisticated controller. Basically, we can implement any kind of controller such as:

$$C(z) = \frac{b_0 + b_1 z^{-1}}{1 + a_1 z^{-1} + a2 z^{-2}} \tag{1}$$

The baseline is to work with a leaky integrator ($b_0 = gain, b_1 = 0, a_1 = -(1 - leak), a_2 = 0$). The leak is a convenient way to avoid the build-up of uncontrolled and unwanted modes. However, the drawback is that the rejection is reduced at low frequency. In Fig.7 (left-side) we show the same transfer functions as in Fig.5, with an increasing leak. As one can see, values of leak greater than 0.005 starts to impact significantly the ETF and should be avoided while in operation. We are also investigating more sophisticated controller like the PI controller (Proportional-Integral) or the Smith predictor. First results obtained on the lab are shown in Fig.7 (right-side). The Smith predictor appears to be an attractive solution, as it provides a somewhat better rejection at low frequency, and a higher bandwidth. These first tests also demonstrates that our theoretical models are accurate as we can reproduce the experimental data with a high precision. These results are only preliminary and more work needs to be done in this direction. Particularly we would like to test on the bench the performance of type II controllers and evaluate the stability and robustness of these controllers.

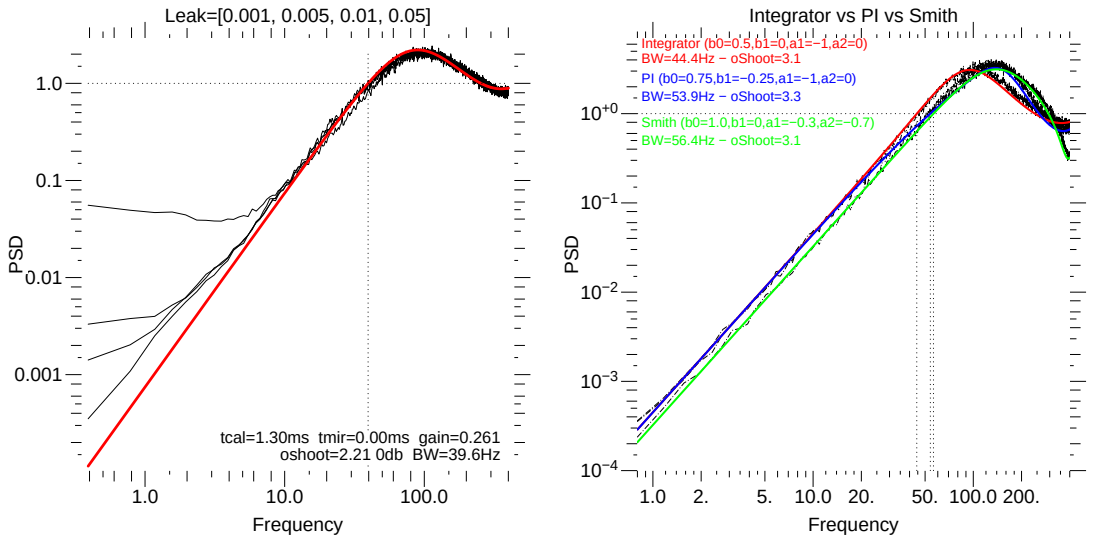

Figure 7. Three examples ETF measured and fitted for DM0.

2.2.2 Tip-Tilt results

The characterization of the TT loop appeared to be crucial as the first measurements revealed an important issue: we evidenced that the computed error was applied one frame latter than it was to supposed to be. Hence the bandwidth was much lower than we expected. After further investigations, we found that the RTC was buffering one frame and we fixed this problem. In Fig. 8 (left panel) we show one of the ETF obtained for the TT loop before the buffered frame issue was fixed. The estimated lag due to computation was then suspiciously too high. In Fig. 8 (center and right panel) we show the same ETF once the issue was fixed. The lag due to calculation is now reduced by one frame, and in agreement with the RTC specifications. We also confirmed that the mirror lag was in good agreement with the constructor data. As for the HO loop, we did a number of calibrations for different gains and loop rates and we found an excellent agreement with the models.

Our experience with Altair show that vibrations and wind-shake can have a major performance impact.[16] Let's consider a (pessimistic) case of telescope wind-shake and guiding errors of 2arcsec peak-to-peak at 1Hz, and an ETF as the ones shown in Fig.8. The residual TT at this frequency would then be around 30mas rms, which would have a major impact on the image quality (remember than 30mas rms means a gaussian kernel of 70mas; twice the diffraction limit at H band). If this really appears to be an issue, we plan to implement a woofer-tweeter scheme for the TT control.[17]

3. DIAGNOSIS TOOLS AND OPTIMIZATION OF THE AO LOOP

While in operation, due to a limitation in the RT design, we cannot have access to every frames of the telemetry data. Instead, we have access to a data stream sent by the RTC at about 30 to 40 frames/s. This data stream

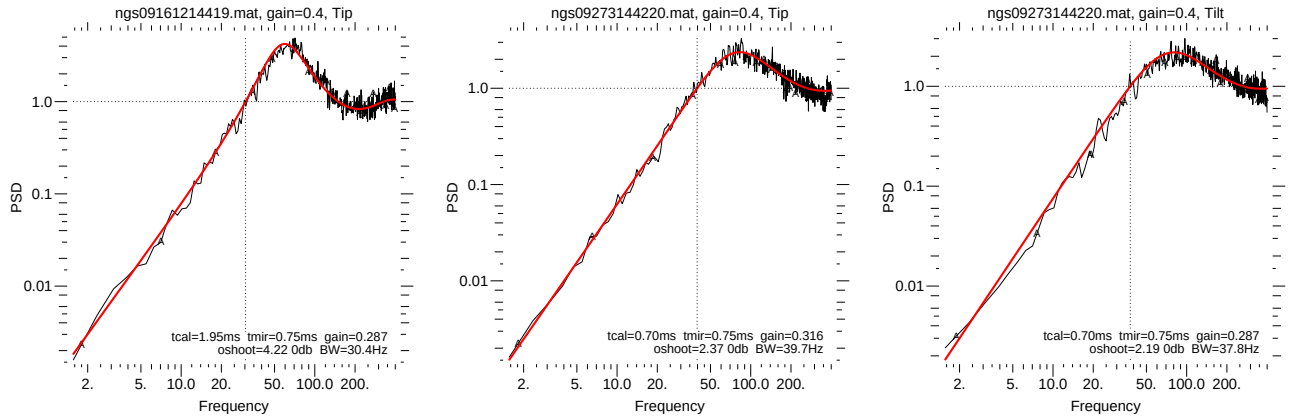

Figure 8. Three examples ETF measured and fitted for the loop TT. The one on the left was measured before the missing frame issue was fixed. The middle and right ones were measured after the fix.

includes many important information like the WFS pixels, slopes, the DM commands, errors and some loop status among other. Based on this data stream we have created a set of tools and real time display screens that allow us to visualize the current state of the loop, follow the general health and performance, and perform statistical analysis. These tools are implemented within Myst, as part of the Real Time Display (RTD) screens and a set of 'Smart tools'. The 'smart tools' are permanently monitoring the status and performance of all the loops and automatically take (smart, but not based on any artificial intelligence concept) decisions and actions according to the external conditions. More details on their implementation and functionality are given in Rigaut et al. companion's paper.[7] On top of the loop monitoring, we make use of the loop statistics in order to evaluate some atmospheric parameters. These atmospheric measurements will permit informed characterization of the performance and will be used to optimize the AO loop (see Sect. 2).

3.1 Loop statistics, Zernike reconstruction, r_0

In Fig.9, we show three Myst RTD screens (among more than 15) to illustrate some of the loop monitoring that are performed in (almost) real time. Basically, all kind of first and second order statistics can be computed on the WFS slopes and DM commands/errors.

Residual slopes and DM commands are projected on Zernike modes. This projection is fitted by a Kolmogorov model to estimate the r_0 parameter. The Zernike coefficients are either estimated from the residual slopes (for open loop operation), the DM commands or both (for close loop operation). The residual slopes of each LGS WFS are also used to derive more statistics (see right-side of Fig.9). Among others, we estimate the static and dynamic projection onto a rotational mode. The static part can be used for alignment purpose while the dynamic part is used to estimate the noise. Indeed, as we do not expect a dynamic rotational mode to be present (this mode can not exist in nature, and the SHWFS lenslet arrays are firmly fixed to the CCDs mechanical structure) , all its contribution can only be due to noise[18] . The residual slopes are also used to compute the residual jitter, and a Strehl Ratio (SR) estimate. The latter can then be scaled by the theoretical SR loss map computed from the NGS constellation/magnitude and used as one of the performance monitoring of the loop.

3.2 Cn2 profiler

We have implemented a Cn2 profiler based on the SLODAR approach.[19–21] The SLODAR method consists in using the spatial covariance of the slopes (phase gradient) measured by N WFS at ground level, each one pointing on a different GS direction.

With GeMS we have 5 high order WFS, each one pointing in a LGS direction, so we make use of these measurements to reconstruct the Cn2 profile. We use all the LGS combinations at the same time, because they

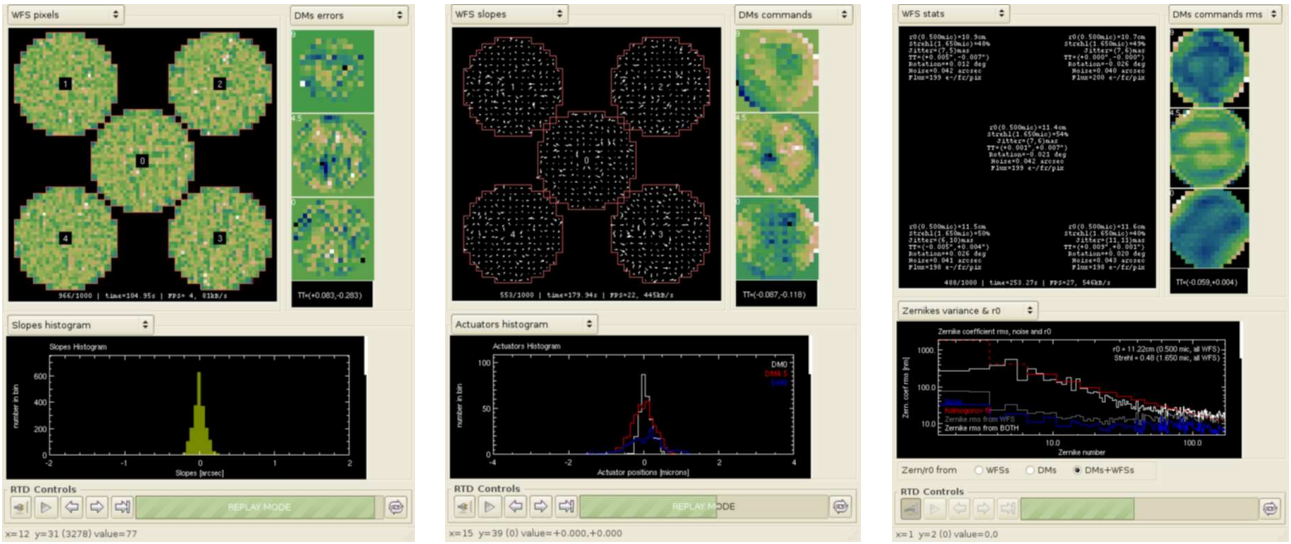

Figure 9. Sample of three Myst RTD screens. *Left:* left panel shows the LGS WFS pixels, right panel the DM errors and bottom panel an histogram of the slopes distribution. *Middle:* left panel show the LGS WFS slopes, right panel the DM commands and bottom panel an histogram of the actuator distribution. *Right:* left panel shows some statistics for each WFS, right panel the DM commands rms and bottom panel the Zernike/r_0 estimation.

all give the same altitude sampling. Each WFS has 16x16 subapertures, so we are reconstructing 16 layers. When the telescope is pointing at zenith, the altitude of these layers is given by:

$$h = \frac{m\ w_0\ z}{z\ \theta + m\ w_0} \tag{2}$$

where m is an integer ranging from 0 to 15, w_0 is the size of the subaperture at the ground level and z is the altitude of the LGS (the latter is updated every 10 seconds as a result of the LGS WFS quad-cell centroid gains calibration procedure). For instance, for an LGS at 90km, the 16 altitudes are: (0, 1666, 3271, 4819, 6313, 7756, 9149, 10496, 11799, 13060, 14281, 15463, 16610, 17721, 18800, 19846)meter. Interestingly, the cone effect makes the bin of altitudes smaller at high altitudes. The altitude sampling also changes when the telescope is pointing at different zenith angle, but as both the LGS altitude and the layer altitudes are changing in the same way, we have decided to correct for this effect and only report the Cn2 profile at zenith.

The SLODAR works with open-loop slopes, so we first need to reconstruct pseudo-open loop data from the close-loop data. To do that, we use the close loop slopes, the commands applied to the DMs, and the interaction matrix. As described in Butterley et al.,[20] we use the Tilt-Tilt filtered slopes to remove telescope guiding errors and wind-shake effects. We also filter the Tip-Tilt signal in the reconstructed open-loop data, as the tilt anisoplanatism modes applied to DM0 and DM9 project in a tilt-combinations on the WFSs. Finally, we take advantage of all the spatial redundancy to compute an averaged slopes correlation matrix, which speeds up the statistical convergence. The slopes correlation matrix is computed as the data are coming and averaged over time. As mentioned above, in operation we only have access to a data stream sent by the RTC at about 30 frames/s. It is this stream that is used to compute the raw covariance matrices. One drawback of this implementation is that we may temporally mismatch the DM commands that are combined with the close-loops slopes by up to a couple frames. However, Monte-Carlo simulations show that this error is negligible, mainly because the DM commands are essentially changing slowly.

In order to fit the above covariance map and be able to evaluate the Cn2 profile, we use a set of covariance maps that correspond to the theoretical response of one layer at one of the altitude given above. The set of theoretical response is constructed from Monte-Carlo simulations that use exactly the same steps as the one used previously. We have tested the algorithm performance with different initial profiles. A sample of the results obtained in simulations are shown in Fig. 10.

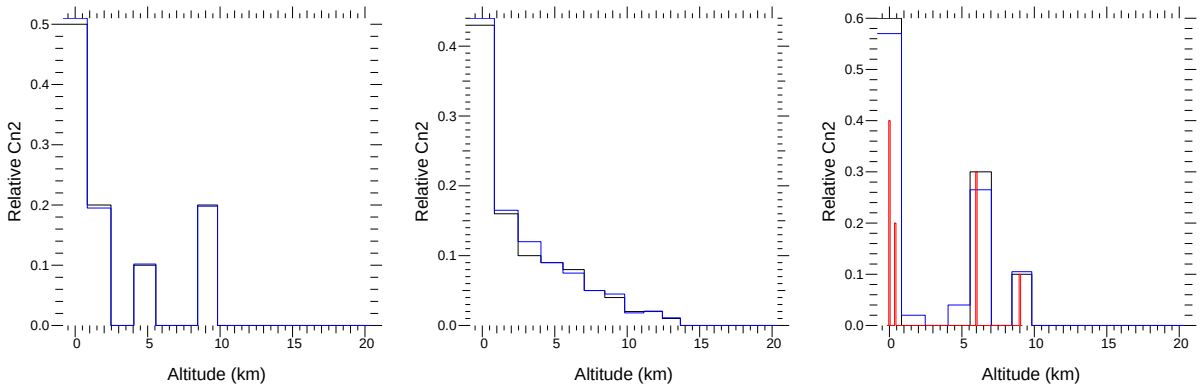

Figure 10. Three examples of reconstructed Cn2 profile from simulations. On the left and middle panels, the original Cn2 profile (black line) exactly matches the theoretical altitudes. The reconstructed Cn2 profile is shown in blue. Respectively 4 and 10 layers are introduced in the original Cn2 profile. In the third panel, the original Cn2 profile is composed of 4 layers that do not match the theoretical altitudes (red line). The black line shows the cumulative Cn2 energy in each reconstructed altitude bins, and the blue line is the reconstructed Cn2 profile. This last example illustrates the effect of the altitude resolution.

We have started to evaluate the error associated with the reconstructed Cn2 profile, and then the observing time required to achieve a given accuracy. The statistical uncertainty associated with the measurements depends on the number of independent samples. As discussed in Butterley et al. this depends on the wind-profile and may vary with altitude. For 'typical' wind profiles observed in Cerro-Pachon (e.g.), we find that an uncertainty better than 10% can be achieved when a new Cn2 profile is published every minute. These values would need to be refined, but they seem reasonable in a first approximation. We have also tried to evaluate the sensitivity of the method to model errors, i.e. when the actual conditions differ from the ones used to compute the theoretical covariance maps. Particularly, we have evaluated that a reasonable error ($< 20\%$) on the LGS WFS centroid gains has only a very small impact ($< 1\%$) on the reconstructed Cn2. This is mainly because most part of the reconstructed open-loop signal comes from the DM commands and not from the slopes. A study of the sensitivity to the outer scale profile L_0 is still pending.

The Cn2 profiler is fully integrated within Myst and working permanently. When GeMS will start on-sky operations, we plan to compare and calibrate the results given by this Cn2 profiler with the ones coming from the MASS/DIMM available at Cerro Pachon.[22]

3.3 Optimization of the AO loop

The loop statistics and atmospheric parameters described above are used to optimize the AO loop during an observation. For instance, depending on the seeing, the flux received on the WFS, the Cn2 profile, we will adjust the loop gains, change the number of corrected modes or the WFS integration time. As it is currently implemented, this optimization relies on Look-Up Tables (LUT), that would need to be optimized during commissioning. During operations, all the telemetry described above and the loop statistics and status are automatically saved. So we plan to start with crude estimates, and continuously improve our models as more and more data are gathered on-sky. In a sense, we are running a continuous optimization of the optimization procedure. The first optimization that we have implemented in Myst is the HO command matrix control: the optimizer automatically compute and load new command matrices depending on the average flux on the LGS WFS, r_0, the Cn2 profile and the noise configuration. We illustrate this process in Fig.11 for a MMSE-like command matrix[23] . On the left-side of Fig.11, we start a simulation with a Cn2 profile made of 4 layers. The 3DMs are used for the MCAO correction. In Fig.11 central-panel, we suddenly change the Cn2 to a ground layer only. Once the Cn2 profiler detects this change, a new command matrix is loaded, and only DM0 is now used for the correction. In Fig.11 right-side, we come back to the original 4layers Cn2 profile, and once this atmospheric change has been detected, the first command matrix is reloaded. We have implemented different command matrix types (Least-Square, Weighted Least-Square, Minimum Mean Square Error, see Neichel et al.[23]) so the optimizer would also have to choose the most appropriate one.

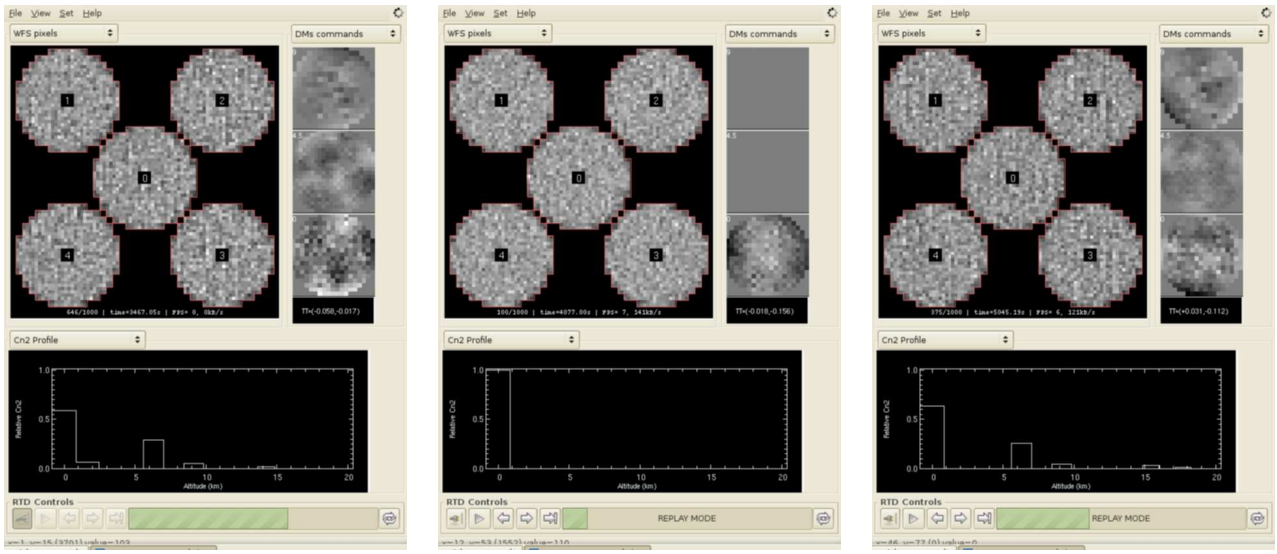

Figure 11. Illustration of the command matrix optimization process when the Cn2 profile evolve over time. *Left:* Cn2 profile is composed of 4layers, the 3DMs are used for the MCAO correction. *Center:* The Cn2 profile suddenly changes to 1 layer at ground, the command matrix is automatically updated to follow this Cn2 evolution. *Right:* The Cn2 conditions come back to the original 4 layers configuration, the 3DMs are used for the correction.

4. VERY FIRST PERFORMANCE EVALUATION IN DYNAMIC

Back in November 2009, we have been able to carry out some preliminary dynamic performance tests on the CANOPUS bench. For that we used the diagnostic camera in the science path, and we looked at the performance while in close loop. Disturbances were introduced by the DMs themselves through turbulent voltages that mimic a Von-Karman turbulence. In Fig.12 we show the PSFs obtained with the test camera at the center of the field for respectively, no disturbances applied, disturbances applied and AO loops open and disturbances applied and AO loops closed. The measured SR is 48% (at 810nm) with no turbulence, and decreases to 34% with turbulence and loop closed. If we translate this result to H band and assuming a better NCPA starting point (e.g. 95%), this would mean that we would be able to reach SR of 90%, at least on the lab. Note that because of the way turbulence is introduced, there is no fitting, MCAO general-fitting nor spatial aliasing error, hence the seemingly large Strehl ratio. Unfortunately, we were able not to pursue this effort because of the AO bench shut-down (see Sect.1.1).

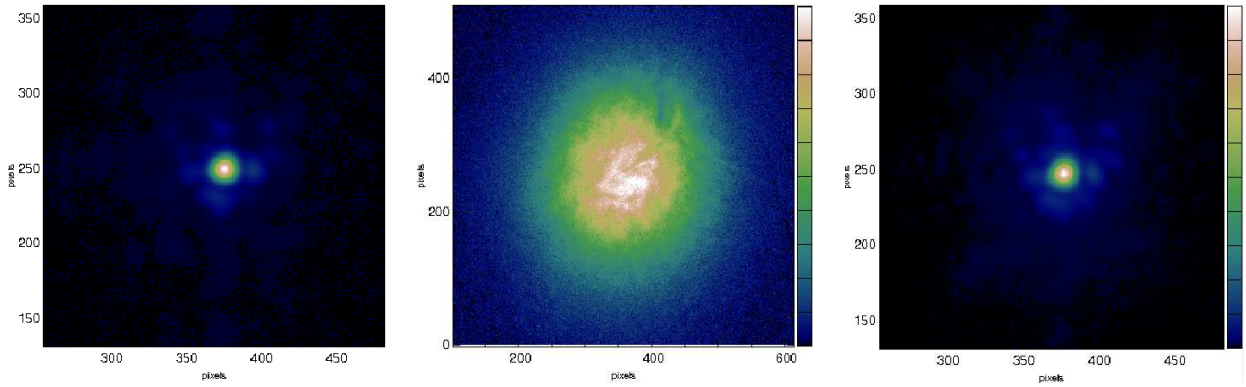

Figure 12. Very first performance results obtained on the CANOPUS Bench. *Left:* Raw PSF, no turbulence, internal SR=48% at 810nm. *Middle:* same, with turbulence, no AO correction. *Right:* AO-corrected PSF, SR=34%.

5. CONCLUSION

As stated in the abstract: "GeMS is a unique and challenging project" and we recently achieved several milestones that make the end of the lab-story a closer reality. The Laser has been delivered to Cerro Pachon and we expect the first propagation at the end of July 2010. Few months from that, the laser and BTO will be ready to accommodate regular operations. CANOPUS has been through a major engineering work to re-design, fabricate and install new cooling enclosures. This effort was the last major engineering work needed to finalize CANOPUS. Integration and AO tests in the lab has revealed many unexpected (and confirmed expected) issues. One interesting example is the loop transfer functions characterization. Indeed, these calibrations show how from simple and basic measurements we finally end-up with trouble shooting issues (DM0 bad actuators and TT loop frame lost) that would have been critical for the final performance. Unfortunately, we faced technical issues (DME incident, DM0 sent for repair) and the bench was out-of-service for close loop operations for almost a year. This prevented us to finalize the AO work and some key tasks (e.g. NCPA) remain in the path. However, we used that opportunity to move a step forward our high-level software tools, which will certainly be crucial for the instrument commissioning and maintenance (e.g. the diagnosis tools, Cn2 profiler, matrix optimization). We currently have one performance issue which is the NGSWFS throughput. Due to design errors and alignment issues, the current setup suffer a 2 magnitude sensitivity loss, which would kill the sky coverage. An effort has started to re-design and test a new NGSWFS setup, that will certainly take several months to finalize. The current plan would be to move CANOPUS to the mountain lab by the end of 2010, and then start the technical commissioning soon after that. This schedule would be optimal as for the more favorable weather conditions during summer time. An instrument shutdown would then be needed during the following winter to retrofit the new NGSWFS and GeMS would finally be offered to the community at the end of 2011.

ACKNOWLEDGMENTS

We want to thanks all the Gemini staff members who are contributing to the GeMS project, both at Gemini North and South. Authors are also grateful to Damien Gratadour for the fruitful collaboration on the phase diversity algorithm. The Gemini Observatory is operated by the Association of Universities for Research in Astronomy, Inc., under a cooperative agreement with the NSF on behalf of the Gemini partnership: the National Science Foundation (United States), the Science and Technology Facilities Council (United Kingdom), the National Research Council (Canada), CONICYT (Chile), the Australian Research Council (Australia), Ministério da Ciência e Tecnologia (Brazil) and Ministerio de Ciencia, Tecnología e Innovación Productiva (Argentina).

REFERENCES

[1] D'Orgeville, C., Daruich, F., and et al., "The gemini south mcao laser guide star facility: getting ready for first light," in [*Adaptive Optics Systems*], Hubin, N., Max, C., and Wizinowich, P., eds., *Proc. SPIE* **7015**, 70152P (2008).

[2] Boccas, M., Rigaut, F., and et al., "Gems: Gemini mcao system, current status and commissioning plans," in [*Adaptive Optics Systems*], Hubin, N., Max, C., and Wizinowich, P., eds., *Proc. SPIE* **7015**, 70150X (2008).

[3] Bec, M., Rigaut, F., and et al., "The gemini mcao bench: system overview and lab integration," in [*Adaptive Optics Systems*], Hubin, N., Max, C., and Wizinowich, P., eds., *Proc. SPIE* **7015**, 701568 (2008).

[4] Rigaut, F., Neichel, B., Bec, M., Boccas, M., Garcia-Rissmann, A., and Gratadour, D., "A sample of gems calibrations and control schemes," in [*1st AO4ELT conference - Adaptative Optics for Extremely Large Telescopes*], Clénet, Y., Conan, J.-M., Fusco, T., and Rousset, G., eds., *EDP Sciences* **1**, 08001 (2010).

[5] Garcia-Rissmann, A., Rigaut, F., Bec, M., Boccas, M., Galvez, R., Gausachs, G., Gratadour, D., and Neichel, B., "Calibration of the mcao canopus bench," in [*1st AO4ELT conference - Adaptative Optics for Extremely Large Telescopes*], Clénet, Y., Conan, J.-M., Fusco, T., and Rousset, G., eds., *EDP Sciences* **1**, 02012 (2010).

[6] Gausachs, G., Bec, M., and Galvez, R., "Chilled water glycol system for canopus at gemini south," in [*Adaptive Optics Systems II*], McLean, I. S., Ramsay, S. K., and Takami, H., eds., *Proc. SPIE* **7735**, 7735–235 (2010).

[7] Rigaut, F., Neichel, B., and et al., "Myst: a comprehensive high-level control tool for gems," in [*Adaptive Optics Systems II*], Ellerbroek, B. L., Wizinowich, P., Hart, M., and Hubin, N., eds., *Proc. SPIE* **7736**, 7736 (2010).

[8] Tracy, A. J., Hankla, A. K., Lopez, C. A., and et al., "High-power solid-state sodium guidestar laser for the gemini north observatory," in [*Solid State Lasers XV: Technology and Devices.*], J., H. H. and K., S. R., eds., *Proc. SPIE* **6100**, 404–415 (2006).

[9] D'Orgeville, C., Arriagada, G., Bec, M., and et al., "Gemini north laser guide star first light," in [*Adaptive Optics*], *Proc. AMOS* (2005).

[10] Wyman, R., Boccas, M., Carter, C., and et al., "Operation and maintenance overview of the gemini north artificial guidestar laser," in [*Adaptive Optics*], *Proc. AMOS* (2007).

[11] Lee, I., Jalali, M., and et al., "20 w and 50 w guidestar laser system update for the keck i and gemini south telescopes," in [*Adaptive Optics Systems*], Hubin, N., Max, C., and Wizinowich, P., eds., *Proc. SPIE* **7015**, 7015N (2008).

[12] Sawruck, N., Lee, I., Jalali, M., and et al., "System overview of 30w and 55w sodium guide stargazer systems," in [*Adaptive Optics Systems II*], Ellerbroek, B. L., Wizinowich, P., Hart, M., and Hubin, N., eds., *Proc. SPIE* **7736**, 7736–69 (2010).

[13] Cavedoni, C. P., Bombino, S., Sheehan, M., and et al., "The gemini mcao infrastructure: Laser service enclosure and support structure," in [*Ground-based and Airborne Telescopes II*], M., S. L. and Roberto, G., eds., *Proc. SPIE* **7012**, 70122Y (2008).

[14] Sauvage, J., Fusco, T., Rousset, G., and Petit, C., "Calibration and precompensation of noncommon path aberrations for extreme adaptive optics," *JOSA-A* **24**, 2334–2346 (2007).

[15] Madec, P., [*Control techniques*], Cambrige University Press (1999).

[16] Christou, J., Neichel, B., Rigaut, F., Sheehan, M., and Trujillo, C., "Altair performance at gemini north," in [*Adaptive Optics Systems II*], Ellerbroek, B. L., Wizinowich, P., Hart, M., and Hubin, N., eds., *Proc. SPIE* **7736**, 7736 (2010).

[17] Veran, J. and Herriot, G., "Woofer-tweeter tip-tilt control for nfiraos on tmt," in [*Advances in Adaptive Optics II*], Ellerbroek, B. L. and Bonaccini Calia, D., eds., *Proc. SPIE* **6272**, 62721R (2006).

[18] Gendron, E. and Léna, P., "Astronomical adaptive optics. 1: Modal control optimization," *A&A* **291**, 337–347 (1994).

[19] Wilson, R., "Slodar: measuring optical turbulence altitude with a shack-hartmann wavefront sensor," *MNRAS* **337**, 103–108 (2002).

[20] Butterley, T., Wilson, R. W., and Sarazin, M., "Determination of the profile of atmospheric optical turbulence strength from slodar data," *MNRAS* **369**, 835–845 (2006).

[21] Vidal, F., Gendron, E., Brangier, M., Sevin, A., Rousset, G., and Hubert, Z., "Tomography reconstruction using the learn and apply algorithm," in [*1st AO4ELT conference - Adaptative Optics for Extremely Large Telescopes*], Clénet, Y., Conan, J.-M., Fusco, T., and Rousset, G., eds., *EDP Sciences* **1**, 07001 (2010).

[22] Wilson, R., Butterley, T., and Sarazin, M., "The durham/eso slodar optical turbulence profiler," *MNRAS* **399**, 21292138 (2009).

[23] Neichel, B., Rigaut, F., Bec, M., and Garcia-Rissmann, A., "Reconstruction strategies for gems," in [*1st AO4ELT conference - Adaptative Optics for Extremely Large Telescopes*], Clénet, Y., Conan, J.-M., Fusco, T., and Rousset, G., eds., *EDP Sciences* **1**, 02010 (2010).